Matter

CellPress

Article

Manipulating Sulfur Mobility Enables Advanced Li-S Batteries

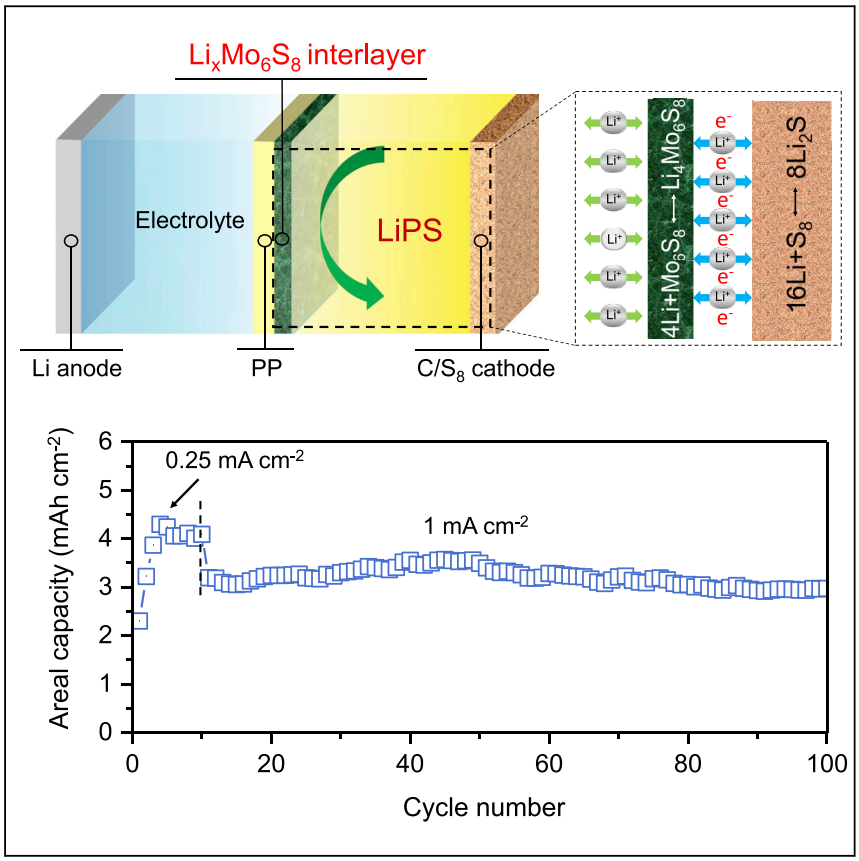

An electrochemically active multifunctional interlayer is developed to overcome some key challenges in lithium-sulfur batteries. The thin interlayer featuring high electronic/ionic conductivities and sufficient catalytic activity effectively prevents the formation of the Li_2S clogging layer and cuts off global sulfur mobilities. Excellent rate capability and cycling stability are achieved. More importantly, it works well with calendered high-sulfur-loading cathodes, significantly improving the volumetric energy density.

Demonstrate
Proof-of-concept of performance with intended application/response

Weijiang Xue, Daiwei Yu, Liumin Suo, ..., Ahmed S. Helal, Wah-Keat Lee, Ju Li

suoliumin@iphy.ac.cn (L.S.)
liju@mit.edu (J.L.)

HIGHLIGHTS

A multifunctional interlayer composed of electrochemically active Mo_6S_8 is developed

It successfully solves the Li_2S clogging problem at the cathode/separator interface

It counteracts cathode-to-anode and within-cathode global sulfur mobilities

It enables calendered high-S-loading cathode and improves volumetric energy density

Xue et al., Matter *1*, 1–14
October 2, 2019
https://doi.org/10.1016/j.matt.2019.07.002

Please cite this article in press as: Xue et al., Manipulating Sulfur Mobility Enables Advanced Li-S Batteries, Matter (2019), https://doi.org/10.1016/j.matt.2019.07.002

Matter

CellPress

Article

Manipulating Sulfur Mobility Enables Advanced Li-S Batteries

Weijiang Xue,[1] Daiwei Yu,[1] Liumin Suo,[1,2,3,4,*] Chao Wang,[1] Ziqiang Wang,[1] Guiyin Xu,[1] Xianghui Xiao,[5] Mingyuan Ge,[5] Minseong Ko,[6] Yuming Chen,[1] Long Qie,[1,7] Zhi Zhu,[1] Ahmed S. Helal,[1] Wah-Keat Lee,[5] and Ju Li[1,8,*]

SUMMARY

Rational design of lithium-sulfur batteries calls for enhancing local sulfur mobility and electrocatalysis while suppressing global sulfur mobility (GSM) from cathode to anode and within cathode without sacrificing volumetric or gravimetric capacities. A multifunctional interlayer composed of electrochemically active Mo_6S_8 with fast topotactic/intercalation reactions, strong lithium polysulfide binding, and high electronic conductivity addresses these challenges. The electrocatalytic $Li_xMo_6S_8$ interlayer successfully solves the harmful stratification by preventing the Li_2S clogging at the cathode/separator interface, thus resulting in a superior rate capability up to 4 C. Remarkably, the $Li_xMo_6S_8$ interlayer works well with the calendered high-loading sulfur cathode with much improved volumetric energy density at a pouch-cell level. An excellent capacity retention with high initial capacity is also achieved with high-sulfur-loading cathode and lean electrolyte.

INTRODUCTION

Lithium-sulfur (Li-S) batteries have attracted much attention due to the high theoretical capacity of the elemental sulfur (1,672 mAh g^{-1}), which is naturally abundant, low in cost, and environmentally friendly.[1] Despite the promising properties, there are two major obstacles to developing practical Li-S batteries. (1) The electronic insulating nature of both end-member phases S_8/Li_2S of the reaction leads to sluggish redox kinetics and limits the capacity utilization. (2) Although the dissolution of intermediate lithium polysulfides (LiPS) in ether-based liquid electrolyte facilitates the kinetics somewhat by allowing the sulfur-containing species to waft to the nearest electron source tens of nanometers away (conductive particles such as carbon black) instead of waiting for the electrons to arrive by polaron conduction (which is very difficult due to the lack of transition metals) or tunneling, a bad side effect of such sulfur mobility is that the LiPS may also transport a much longer distance (such as tens of micrometers), for example across the electrolyte to the Li anode side ("shuttling"), which will result in the loss of both Li and S and, thus, a poor cycle life.[2]

To address these issues, much effort has been expended on building smart cathode architectures by introducing LiPS adsorbing materials[3–6] or binders[7,8] serving as sulfur hosts. The ideal scenario is to have high local sulfur mobility within a tens-of-nanometers local region of the cathode to enable fast redox, but low global sulfur mobility (GSM) across tens-of-micrometers distance—the worst kind of GSM being that of crossing over from cathode side to the anode side. This calls for effective approaches of constructing a membrane between the traditional separator and cathode (the so-called interlayer[9,10]) to eliminate cathode-to-anode GSM.

Progress and Potential

Lithium-sulfur batteries have attracted tremendous interest due to the high theoretical specific capacity, low cost, and environmental friendliness of the elemental sulfur compared with the transition metal-based conventional Li-ion batteries, but it still faces major challenges on the cathode side. The key to solving the challenges is to have high local sulfur mobility within a tens-of-nanometer local region of the cathode to enable fast redox, but low global sulfur mobility (GSM), across tens-of-micrometer distance to suppress the shuttling effect and prevent the Li_2S clogging without compromising energy density. This work presents an effective strategy to manipulate the sulfur mobility by an electrochemically active multifunctional $Li_xMo_6S_8$ interlayer. The interlayer successfully suppresses the GSM, leading to a superior rate capability, and enables a calendered high-sulfur-loading cathode with improved volumetric energy density and excellent cycling stability at a pouch-cell level.

Please cite this article in press as: Xue et al., Manipulating Sulfur Mobility Enables Advanced Li-S Batteries, Matter (2019), https://doi.org/10.1016/j.matt.2019.07.002

Furthermore, such a "smart" membrane should also be more effective at regulating the properties of the cathode/separator interface. A less discussed, but potentially harmful consequence of GSM is stratification. The sulfur cathode is a fragile, porous body, typically 100 μm thick. Even though when made the composite may have a nearly uniform composition and microstructure, it is conceivable that with cycling it can develop heterogeneous layering in the thickness direction, with gradients in volume fractions of S_8, Li_2S, carbon phases, porosity, and electrolyte. Since the $S_8 \leftrightarrow Li_2S$ transformation involves large volume changes, the initial porosity distribution and the fragile carbon black chains that support percolating electronic transport may be changing in this semi-fluid, semi-solid body. In particular, it is not inconceivable that a "dead layer" of Li_2S or S_8, devoid of necessary porosity or electrocatalytical surface areas that support the essential electronic and ionic conductivities, may develop during cycling, leading to poor rate performance and capacity fading. Through continuum-scale modeling,[11] it has been shown that stratification and a dead layer of Li_2S may indeed form near the separator if no special cell design is implemented. This again calls for a "smart" membrane to prevent the formation of the Li_2S clogging layer on the cathode side of the separator. In other words, this membrane should not only cut off cathode-to-anode GSM but should also heal the bad effect of GSM within the cathode, by being both electronically conductive and electrocatalytically active.

Previously, carbonaceous interlayers[12–14] have received considerable attention because of their large specific surface area and high electrical conductivity; however, the weak interactions between the polar LiPS and non-polar carbon undermine their utility as LiPS traps.[15,16] To achieve stronger adsorption for LiPS, new materials with strong chemical binding with LiPS, such as metal oxides,[17–20] metal sulfides,[21] metal-organic frameworks (MOFs),[22,23] and inorganic/organic composite,[21–26] have been explored as new materials for interlayers. However, the insulating nature of those materials impedes electronic transport, resulting in low sulfur utilization and large polarization. More recently, electronically conductive polar materials[27–31] have been incorporated into sulfur cathodes, which could be promising candidates for constructing electronically conductive interlayers. However, all the interlayers above are non-active in terms of lithiation capacity in the voltage range of interest and sacrifice gravimetric energy density (E_g) and volumetric energy density (E_v).[32–34] Although calendering tends to improve the E_v of most lithium-ion battery (LIB) cathodes, it degrades the performance of most sulfur cathodes produced thus far.[35] Therefore, a comprehensive strategy is needed to solve the challenges in Li-S batteries without compromising the practical E_g and E_v.

In the present work, a thin and lightweight interlayer has been constructed using electrochemically active Mo_6S_8 with fast intercalative Li transport,[6] which is demonstrated through coating Mo_6S_8 on Celgard polypropylene separator (PP@$Li_xMo_6S_8$). This greatly suppresses GSM and thus results in remarkable cycling stability (Figure 1A). Unlike all the reported non-active materials[9,13,17–26,36–40] for interlayers, Mo_6S_8 exhibits low electronic resistance[6] and additional capacity contribution in ether-based electrolyte (Figure 1A). Benefiting from the aforementioned unique properties, the PP@$Li_xMo_6S_8$ successfully addresses the Li_2S clogging issue at the cathode/separator interface, resulting in an excellent rate capability up to 4 C. Remarkably, the $Li_xMo_6S_8$ interlayer works well with the calendered high-sulfur-loading cathode with much improved E_g and E_v. An areal capacity >2.9 mAh cm^{-2} with an excellent retention of 93.1% over 100 cycles is realized. Furthermore, a pouch cell using lean electrolyte condition (electrolyte to S_8 ratio, E/S ~ 3.3 μL mg^{-1}) exhibits high initial capacity of 1,205 mAh g^{-1} with > 90% retention over 39 cycles.

[1]Department of Nuclear Science and Engineering, Department of Materials Science and Engineering and Department of Electrical Engineering and Computer Science, Massachusetts Institute of Technology, Cambridge, MA 02139, USA

[2]Beijing Advanced Innovation Center for Materials Genome Engineering, Key Laboratory for Renewable Energy, Beijing Key Laboratory for New Energy Materials and Devices, Beijing National Laboratory for Condensed Matter Physics, Institute of Physics, Chinese Academy of Sciences, Beijing 100190, China

[3]Center of Materials Science and Optoelectronics Engineering, University of Chinese Academy of Sciences, Beijing 100049, China

[4]Songshan Lake Materials Laboratory, Dongguan, Guangdong 523808, China

[5]National Synchrotron Light Source II, Brookhaven National Laboratory, Upton, NY 11973, USA

[6]Department of Metallurgical Engineering, Pukyong National University, Busan 48547, Republic of Korea

[7]Institute of New Energy for Vehicles, School of Materials Science and Engineering, Tongji University, Shanghai 201804, China

[8]Lead Contact

*Correspondence: suoliumin@iphy.ac.cn (L.S.), liju@mit.edu (J.L.)

https://doi.org/10.1016/j.matt.2019.07.002

Please cite this article in press as: Xue et al., Manipulating Sulfur Mobility Enables Advanced Li-S Batteries, Matter (2019), https://doi.org/10.1016/j.matt.2019.07.002

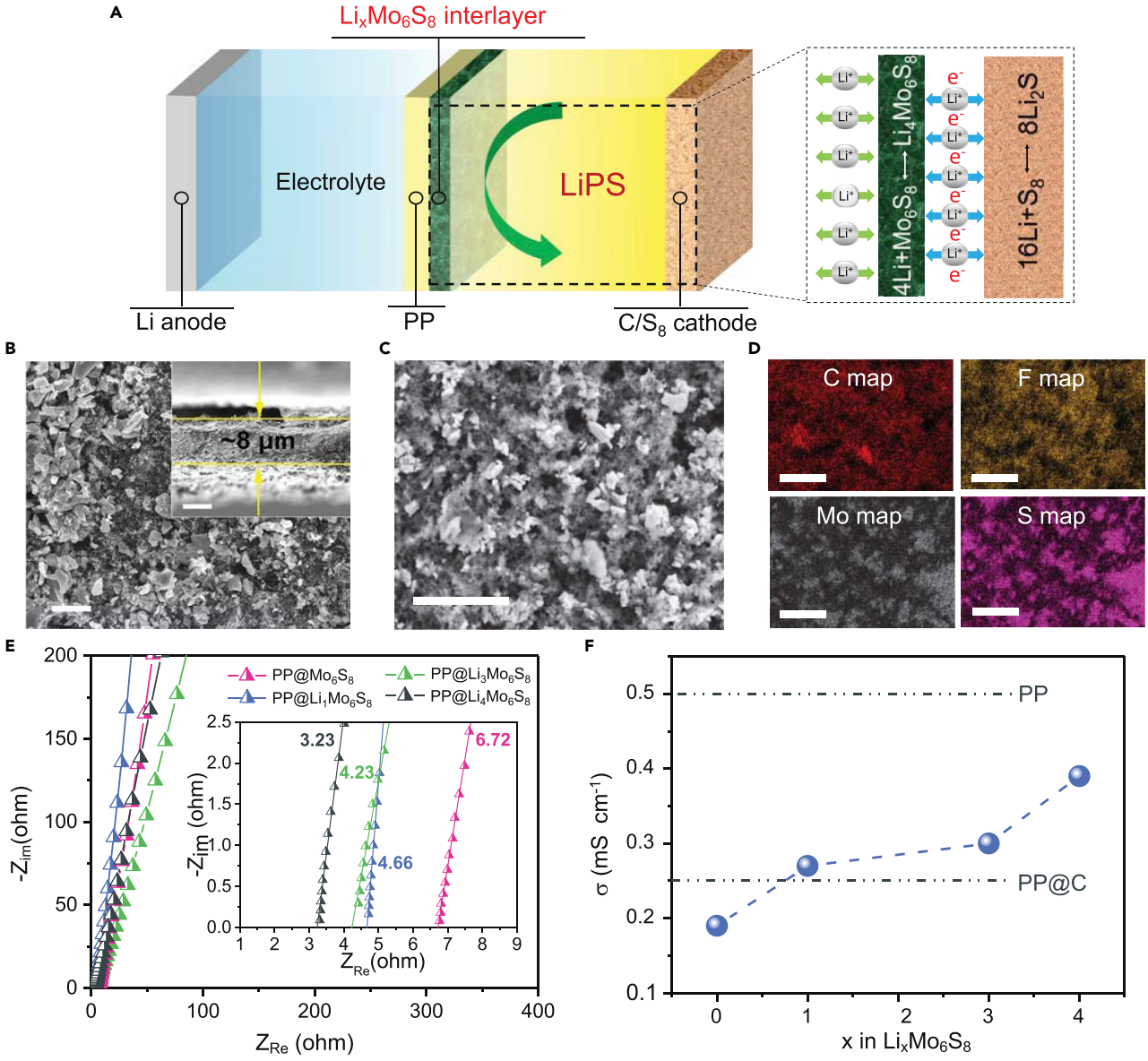

Figure 1. Schematic Illustration and Characterizations of the PP@$Li_xMo_6S_8$ in Li-S Batteries

(A) Schematic illustration of the multifunctional $Li_xMo_6S_8$ interlayer suppressing LiPS shuttling, contributing additional capacity and preventing Li_2S clogging.

(B) The surface and cross-sectional (inset) SEM observations of the PP@$Li_xMo_6S_8$. Scale bars, 1 μm (main panel) and 5 μm (inset).

(C and D) SEM micrograph (C) and corresponding elements distribution (D) of the PP@$Li_xMo_6S_8$ after cycling for 300 cycles at fully charged state. Scale bars, 5 μm.

(E and F) Electrical impedance (E) and ionic conductivity σ (F) of PP@Mo_6S_8, PP@$Li_1Mo_6S_8$, PP@$Li_3Mo_6S_8$, and PP@$Li_4Mo_6S_8$.

RESULTS AND DISCUSSION

Mo_6S_8 was fabricated by leaching Cu from $Cu_2Mo_6S_8$ based on a solid-state method.[41] The as-obtained Mo_6S_8 is rhombohedral (JCPDS: 82-1709, Figure S1). A mixture of Mo_6S_8 and conductive carbon black was coated to form a uniform and dense layer on the PP separator surface (Figure 1B). For high energy densities, the coating layer should be as thin and light as possible. In this work, the small thickness (~8 μm) and light weight (0.4 mg cm^{-2}) of the Mo_6S_8 coating are comparable with the best reports so far (Table S1).

Please cite this article in press as: Xue et al., Manipulating Sulfur Mobility Enables Advanced Li-S Batteries, Matter (2019), https://doi.org/10.1016/j.matt.2019.07.002

For an electrochemically active interlayer, a good compatibility with ether-based electrolyte is necessary. Mo_6S_8 features high polaron conductivity and open lattice structure that allows fast Li transport, which attracts much attention in aqueous batteries.[41,42] Figure S2 shows a typical cyclic voltammogram (CV) profile of Mo_6S_8 in 1 M LiTFSI in 1,3-dioxolane/dimethoxyethane (DOL/DME) electrolyte with 2 wt % $LiNO_3$ within 1.7–2.8 V. Reduction peaks represent the transformation from Mo_6S_8 to $Li_xMo_6S_8$ (x = 1, 3, 4), which is identical to the redox reaction in aqueous electrolyte. In addition, Mo_6S_8 exhibits very good rate capability in ether-based electrolyte, indicative of very fast Li-intercalative reaction kinetics (Figure S3). All these results indicate good compatibility of $Li_xMo_6S_8$ with the ether-based electrolyte.

A series of electrochemical measurements were conducted to evaluate the influence of the Mo_6S_8 layer on separator properties. Overall ionic conductivity was measured by electrochemical impedance spectroscopy (EIS) in a symmetrical stainless steel (SS) two-electrode device (Figure 1E). The electrochemically active features of interlayers at different lithiation levels, namely, PP@Mo_6S_8, PP@$Li_1Mo_6S_8$, PP@$Li_3Mo_6S_8$, and PP@$Li_4Mo_6S_8$, were tested with the pristine PP separators and carbon-coated PP (PP@C) for comparison. The corresponding ionic conductivities were also calculated based on EIS data (Figure 1F). As we know, the pristine separator plus the interlayer usually slows down Li^+ transport. In contrast, notably, with the lithiation of Mo_6S_8 its corresponding ionic conductivity increases from 0.19 to 0.39 mS cm^{-1}, higher than that of the PP@C (0.25 mS cm^{-1}) while lower than the pristine PP separator (0.51 mS cm^{-1}). Furthermore, the Li^+ diffusion coefficients ($D_{Li}{}^+$) of batteries employing the PP@$Li_xMo_6S_8$ and PP@C were calculated from a series of CVs at different scan rates (Figures S4A and S4B; Table S2). The linear fit of the peak current at different scan rates (Figure S4C) indicates a diffusion-controlled process. It is worth noting that $D_{Li}{}^+$ values of the cell employing PP@$Li_xMo_6S_8$ are higher than those using the PP@C and similar to those using a bare separator ($D_{Li}{}^+ = 2 \times 10^{-8}$ to 9×10^{-9} cm^2 s^{-1}),[36] suggesting the diffusion from the sulfur cathode side to the anode side without much additional impediment.

Unlike non-active interlayers, one may be concerned about how an electrochemically active interlayer that has large volume change during lithiation-delithiation would affect the interlayer/cathode interface. To shed more light on this, we performed *in situ* 3D tomography on the pouch cell with PP@$Li_xMo_6S_8$ using synchrotron-based full-field X-ray imaging (FXI), which is a powerful tool to monitor the microstructural evolution in real batteries. Figure 2 presents the reconstructed 3D tomography figures of a box with dimensions 14.70 μm × 11.55 μm × 3.15 μm of the Mo_6S_8 particles at fully charged and discharged states. Figures 2A and 2B match well with each other despite some small volume expansion after full discharge,[43] indicating good structural stability of the PP@$Li_xMo_6S_8$. In addition, we also performed its stability evaluation after long-term cycling. The X-ray diffraction (XRD) pattern (Figure S5) and high-resolution transmission electron microscopy (TEM) image (Figure S6) of the $Li_xMo_6S_8$ after 300 cycles reveal that Mo_6S_8 maintains the crystalline rhombohedral phase well, indicating good long-term structural stability. Furthermore, we note from the elemental mapping after cycling (Figures 1C and 1D) that the distribution of S is in accordance with that of Mo, demonstrating the favorable adsorption capability of sulfur species by $Li_xMo_6S_8$.

Batteries with PP@$Li_xMo_6S_8$, PP@C, and pristine PP were evaluated at different current densities. By comparing with PP@C and pristine PP (Figure S7), the battery with PP@$Li_xMo_6S_8$ exhibits voltage profiles with obvious extra charge/discharge plateaus between 2.4 and 2.5 V in addition to the characteristic plateaus of S_8 (Figure 3A),

Please cite this article in press as: Xue et al., Manipulating Sulfur Mobility Enables Advanced Li-S Batteries, Matter (2019), https://doi.org/10.1016/j.matt.2019.07.002

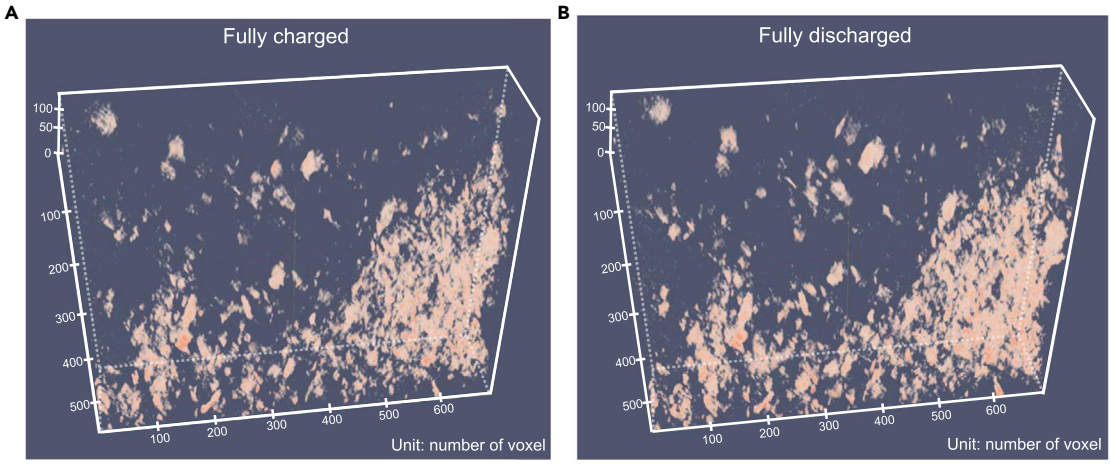

Figure 2. *In Situ* 3D Tomography

In situ 3D tomography of Mo_6S_8 Particles on the PP@$Li_xMo_6S_8$ before (A) and after (B) discharging to 1.7 V using the FXI beamline at National Synchrotron Light Source II, Brookhaven National Laboratory. Voxel size is 21 nm, corresponding to a 3D box of 14.70 μm × 11.55 μm × 3.15 μm.

revealing the additional capacity contribution from $Mo_6S_8 \leftrightarrow Li_1Mo_6S_8$. More importantly, even at higher rates of 3 C and 4 C, the battery with the PP@$Li_xMo_6S_8$ still maintains long and flat discharge plateaus, while those with PP@C and PP have much larger polarization and much lower discharge capacities (Figure S7). Such faster redox reaction kinetics by employing PP@$Li_xMo_6S_8$ compared with the PP@C and PP can be further illustrated by the calculated polarization at various C-rates (Figure S8). Although the PP@C exhibits smaller polarization than the pristine PP separator, its rate performance is still very poor especially at higher rates. Remarkably, the battery with the PP@$Li_xMo_6S_8$ exhibits excellent rate performance, delivering high reversible capacities of 1,409 mAh g^{-1} (0.2 C), 1,206 mAh g^{-1} (0.5 C), 1,074 mAh g^{-1} (1 C), 929 mAh g^{-1} (2 C), 818 mAh g^{-1} (3 C), and 728 mAh g^{-1} (4 C) (Figure 3B). This proves that the $Li_xMo_6S_8$ interlayer is beneficial for improving the redox kinetic of C/S_8 electrode. Mo_6S_8 is obviously much better than carbon due to its unique properties of strong interaction with LiPS and good ionic/electronic conductivities.

The effect of different interlayers on the electrochemical kinetics at the battery level was investigated by EIS to further elucidate the mechanism of the enhanced kinetics. The Nyquist plots of batteries using the PP@$Li_xMo_6S_8$ and PP@C before cycling are shown in Figure 3C. An equivalent circuit was used to fit Nyquist plots consisting of an ohmic resistance of the electrolyte solution (R_s) with one or more resistance//constant phase elements (R//CPE) and a Warburg element (W).[44] Excellent fitting can be achieved when employing the equivalent circuit in Figure 3C (inset), indicating two semicircles in the high-frequency region—a charge-transfer resistance R_{ct} and an interface contact resistance between the coating layer and cathode R_{int}. The R_{int} from the battery using the PP@$Li_xMo_6S_8$ (38.7 Ω) is much smaller than that from the battery using the PP@C (175 Ω), implying a much faster Li^+ diffusion between the $Li_xMo_6S_8$ layer and the sulfur cathode (Table S3). After discharging to 1.7 V for the first cycle, the conversion of the LiPS to the solid Li_2S film on the cathode surface results in large interface contact resistance R_{sl} in the low-frequency region (Figure 3D). Notably, the R_{sl} from the battery using the PP@$Li_xMo_6S_8$ (97.9 Ω) is one order of magnitude smaller than that from the cell using the PP@C (1,106 Ω). Such smaller resistances can be further confirmed by monitoring the EIS plots after 100 cycles (Figures S9 and S10).

Please cite this article in press as: Xue et al., Manipulating Sulfur Mobility Enables Advanced Li-S Batteries, Matter (2019), https://doi.org/10.1016/j.matt.2019.07.002

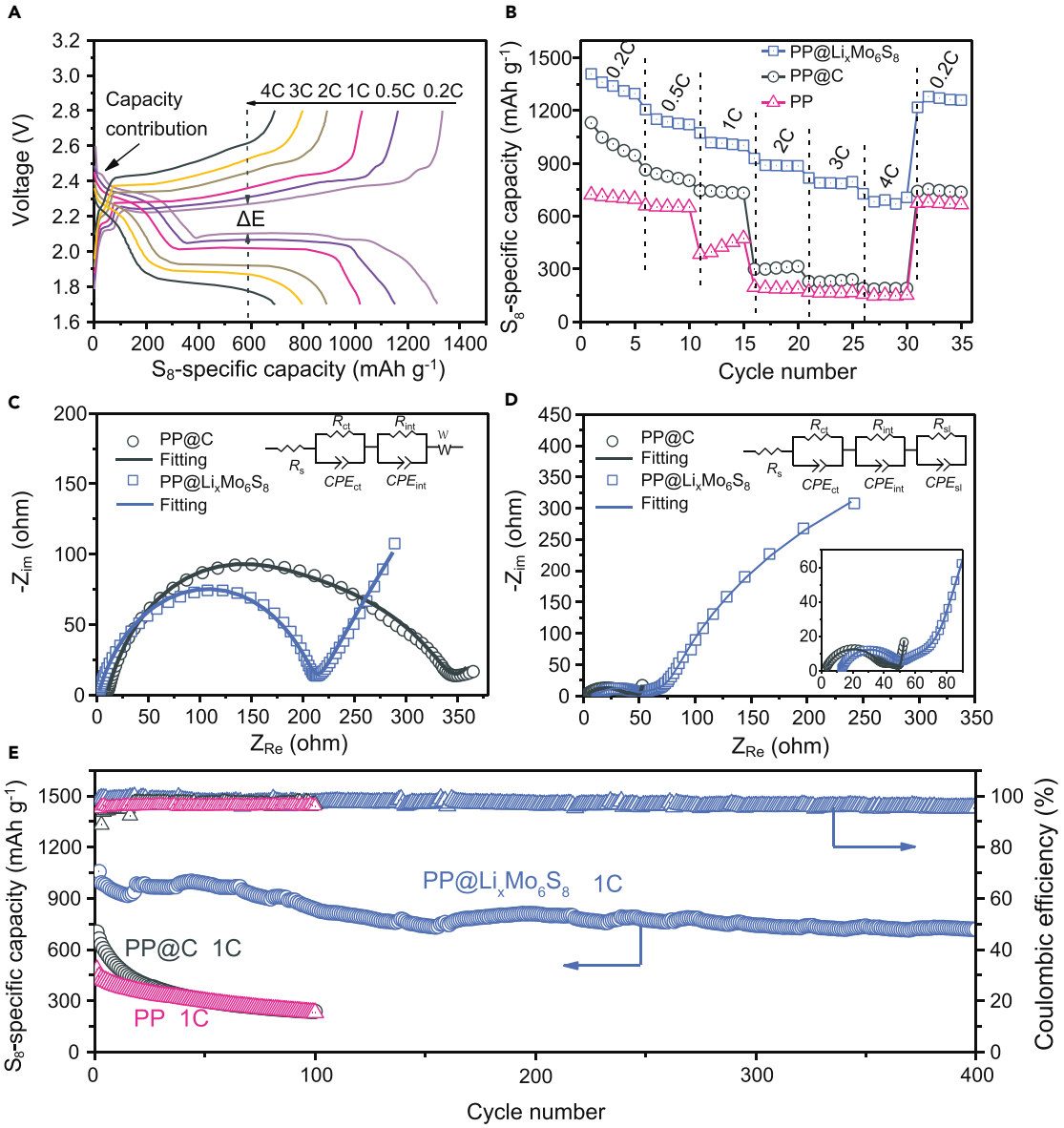

Figure 3. Electrochemical Performances of Li-S Batteries

(A) Voltage profiles at various rates from 0.2 C to 4 C with the PP@$Li_xMo_6S_8$.

(B–D) Rate performances at various rates from 0.2 C to 4 C with the PP@$Li_xMo_6S_8$, PP@C, and pristine PP (B). EIS plots of Li-S batteries before cycling (C) and after first discharge (D).

(E) Cycling performance at 1 C over 400 cycles with PP@$Li_xMo_6S_8$, PP@C, and pristine PP separators. All the specific capacities are based on the S_8 weight only. The specific capacity based on S_8 + interlayer weight (with conductive agents, binders, and Mo_6S_8) will be 22%–25% lower.

The greatly improved redox kinetics could be attributed to another unique benefit of our PP@$Li_xMo_6S_8$: preventing Li_2S clogging. The formation of a Li_2S clogging layer without requisite porosity or conductive agents dispersed inside upon discharging is considered a critical reason leading to poor rate capability of Li-S batteries.[1,11] As mentioned in the Introduction, it is a bad side effect of within-cathode GSM. Although such a "dead layer" at the cathode surface could be avoided via the carbon interlayer (Figure S11A), its formation on the carbon interlayer/separator interface cannot be avoided (Figures 4A and S12), leading to underutilized sulfur and poor rate performance. However, surprisingly our $Li_xMo_6S_8$ interlayer successfully

Please cite this article in press as: Xue et al., Manipulating Sulfur Mobility Enables Advanced Li-S Batteries, Matter (2019), https://doi.org/10.1016/j.matt.2019.07.002

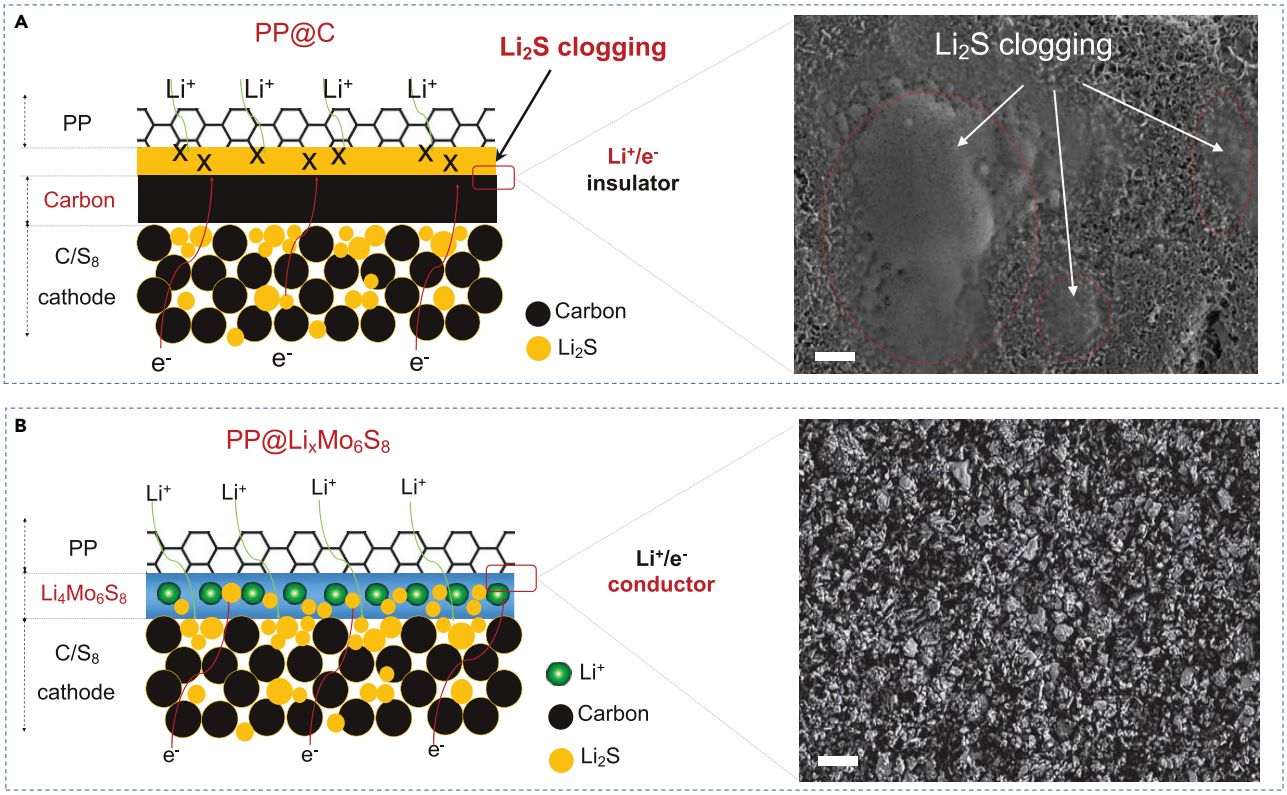

Figure 4. The Different Roles Played in Preventing Li_2S Clogging by PP@C and PP@$Li_xMo_6S_8$

The formation of the Li_2S clogging by PP@C (A) and PP@$Li_xMo_6S_8$ (B) showing that the PP@$Li_xMo_6S_8$ can successfully prevent the Li_2S clogging due to its high LiPS adsorption capability and good ionic and electronic conductivities, while PP@C cannot prevent the Li_2S clogging. SEM images of the surface of the carbon interlayer and $Li_xMo_6S_8$ interlayer attached to the Celgard PP separator at fully discharged state are included in (A) and (B), respectively. Scale bars, 5 μm.

prevents Li_2S clogging both at the cathode surface (Figure S11B) and the $Li_xMo_6S_8$/separator interface (Figure 4B). The energy-dispersive X-ray spectroscopy mapping of element S on the fully discharged cathode surface clearly indicates a very uniform distribution of the discharge product Li_2S (Figure S13). Compared with the carbon interlayer, which only provides good electronic conductivity, the electrochemically active Mo_6S_8 interlayer has not only high electronic and ionic conductivities but also sufficient catalytic activity to "reactivate" the Li_2S inside the $Li_4Mo_6S_8$ layer upon increasing voltage. Thus, a smothering Li_2S clogging layer never gets to form, and the Li_2S products of reduction always maintain the proper size, porosity, and access to electrocatalytic surface and free electrons and ions, minimizing loss of the active material.

To evaluate the long-term cycling performance, we tested batteries with PP@$Li_xMo_6S_8$, PP@C, and pristine PP by galvanostatic charge-discharge measurement. Notably, the battery using PP@$Li_xMo_6S_8$ delivers the highest initial capacities of 1,056 mAh g^{-1} and exhibits excellent long-term cyclability with high capacity retention of 69% at 1 C after 400 cycles (Figure 3E), demonstrating that the PP@$Li_xMo_6S_8$ not only effectively confines LiPS inside the cathode but also "reactivates" it during long-term cycling. In comparison, batteries with PP@C and PP separator show not only much lower capacities but also poor cycling stability (Figure 3E). In addition, we found that a denser Mo_6S_8 layer is beneficial for long-term cycling stability, which is also preferable for improving the volumetric energy density

Please cite this article in press as: Xue et al., Manipulating Sulfur Mobility Enables Advanced Li-S Batteries, Matter (2019), https://doi.org/10.1016/j.matt.2019.07.002

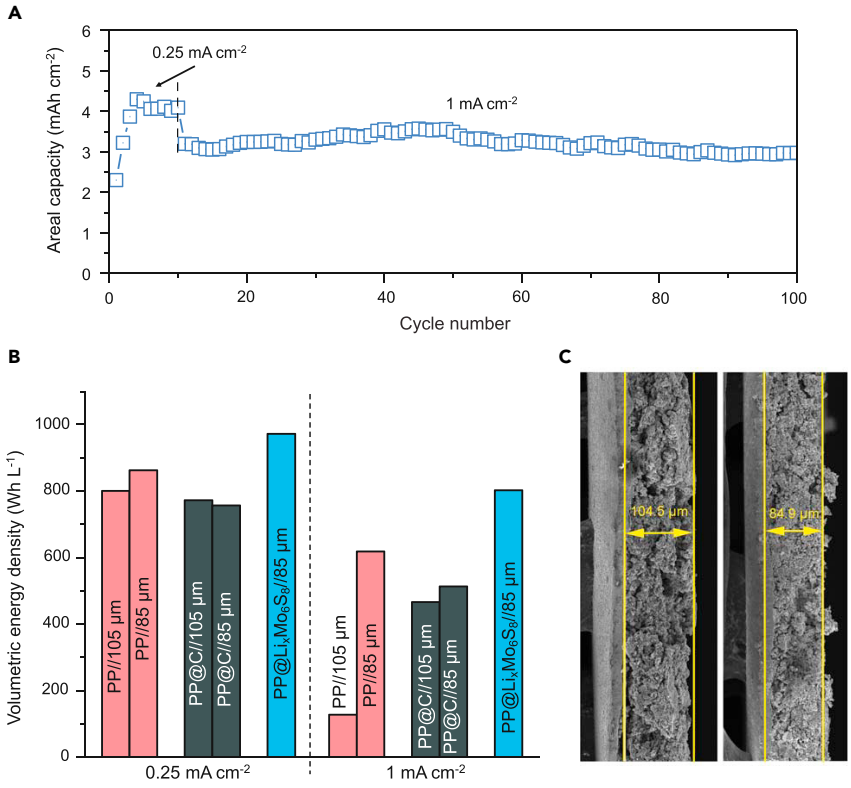

Figure 5. Cycling Performance and Volumetric Energy Density of the High-Loading Cathodes

(A) Areal capacity at current densities of 0.25 and 1 mA cm^{-2} of the Li-S battery with the PP@$Li_xMo_6S_8$ using a calendered high-sulfur-loading (4.02 mg cm^{-2}) cathode.

(B and C) Volumetric energy densities (B) of rolled and unrolled cathodes by employing PP@$Li_xMo_6S_8$, PP@C, and pristine PP separator at 0.25 and 1 mA cm^{-2} (both the cathode and interlayer volumes are taken into account). (C) SEM images of C/S_8 electrodes before (~105 μm) and after (~85 μm) rolling.

(Figure S14). The low-C-rates cycling test, which is very challenging for Li-S batteries, was also conducted to demonstrate the effect of PP@$Li_xMo_6S_8$ on cycle life (Figure S15). The battery using the PP@$Li_xMo_6S_8$ exhibits high capacity retention of 71.9% over 250 cycles compared with the much poorer retention of only 38.2% for the battery using the PP@C. Furthermore, the battery with blank PP has the lowest Coulombic efficiency (CE) while that with PP@$Li_xMo_6S_8$ exhibits the highest CE of up to 99.6% (Figure S16). These results indicate that the $Li_xMo_6S_8$ interlayer is effective in suppressing GSM and thus improving the cycling stability.

To further demonstrate the efficacy of PP@$Li_xMo_6S_8$, we evaluated a calendered high-sulfur-loading electrode (>4.0 mg cm^{-2}). As shown in Figure 5A, upon cycling at 0.25 mA cm^{-2} a discharge capacity of 4.3 mAh cm^{-2} was obtained after the initial activation, corresponding to a specific capacity of 1,070 mAh g^{-1}. As the current density increased to 1 mA cm^{-2}, the areal capacity can be stabilized at above 2.9 mAh cm^{-2} over 100 cycles with extremely high capacity retention of 93.1%, indicating that the $Li_xMo_6S_8$ interlayer is an effective approach for Li-S batteries to improve cycling stability at industrial-level sulfur loading.

Although Li-S batteries are known for very promising E_g, their E_v is not competitive with LIBs[32] owing to the high electrode porosity of most sulfur cathodes, which

Please cite this article in press as: Xue et al., Manipulating Sulfur Mobility Enables Advanced Li-S Batteries, Matter (2019), https://doi.org/10.1016/j.matt.2019.07.002

significantly hinders their potential applications. There may be some concerns about the additional volume after adopting separator modifications or interlayers, which could make E_v even lower than before adoption. However, this is not the case for our $Li_xMo_6S_8$ interlayer. First of all, the electrochemically active Mo_6S_8 shows a respectable volumetric capacity (Note S1). More importantly, thanks to the enhancement in reaction kinetics by the $Li_xMo_6S_8$ interlayer, higher E_v can be achieved by successfully utilizing a high-loading as well as denser C/S_8 electrode.

Calendering (pressurized rolling) is a highly effective process for LIB cathodes to decrease the electrode porosity and increase E_v, but this was historically not true for Li-S cathodes because denser sulfur electrode usually leads to a more severe Li_2S clogging issue and, thus, poor rate performance and larger polarization.[35] Here, after rolling, the thickness of our high-loading C/S_8 electrode decreases from 105 μm to 85 μm (Figure 5C). Therefore, compared with traditional Li-S batteries constructed with the unrolled 105-μm cathode and the PP separator, the increase in thickness by adopting the Mo_6S_8 interlayer (8 μm) can be easily offset by the electrode thickness decrement (20 μm). With just the PP separator or PP@C, the 85-μm-thick denser electrode shows poor rate capability and cyclability (Figure S17). In contrast, the 85-μm calendered electrode paired with PP@$Li_xMo_6S_8$ exhibits very high capacity of > 3 mAh cm^{-2} at 1 mA cm^{-2} (Figure 5A), suggesting that the $Li_xMo_6S_8$ interlayer is very good at improving the rate capability and facilitating the redox kinetics of the denser cathode. As shown in Figure 5B, we calculated the E_v values for rolled and unrolled cathodes with the PP, PP@C, and PP@$Li_xMo_6S_8$ (Note S1). Notably, for the 85-μm calendered electrode, E_v with the PP@$Li_xMo_6S_8$ is ~1.21-fold and ~5-fold that with the PP separator at 0.25 and 1 mA cm^{-2}, respectively. The cycling performance is also greatly improved by employing PP@$Li_xMo_6S_8$.

To further demonstrate the good performances of the $Li_xMo_6S_8$ interlayer in reality, we evaluated a pouch cell (Figures 6A and 6B) by employing a calendered high-loading cathode with a higher sulfur content (62 wt % in cathode, 58.3 wt % in cathode + interlayer) and lean electrolyte (3.3 μL mg^{-1}_{S8} or 3 μL $mg^{-1}_{(S8+Mo6S8)}$). After calendering, the cathode thickness decreases from 120.6 μm to 100.5 μm (Figures S18C and S18D). Figure 6C shows the cycling performance of pouch cells using the rolled cathodes and separators with/without the $Li_xMo_6S_8$ interlayer at 0.2 C. The pouch cell using PP@$Li_xMo_6S_8$ delivers a high S_8-specific capacity of 1,205 mAh g^{-1}, or 1,114 mAh g^{-1} based on S_8 + Mo_6S_8 weight, with > 90% retention after 39 cycles. In sharp contrast, the pouch cell with the PP separator only exhibits a lower specific capacity of 947 mAh g^{-1}_{S8} after nine activation cycles but decays quickly afterward. The specific capacity and cycling stability of the unrolled cathode with the PP separator (Figure S19) are still much worse than the one with the $Li_xMo_6S_8$ interlayer, which can work well with the ~20 μm thinner cathode. These results further demonstrate that the $Li_xMo_6S_8$ interlayer is effective in improving both the sulfur utilization and cycling stability.

Conclusion

We have developed an electrochemically active multifunctional $Li_xMo_6S_8$ interlayer for Li-S batteries, simultaneously equipped with superior electronic and ionic conductivities, extra capacity contribution, and the ability to catalyze and prevent Li_2S clogging. The battery with the PP@$Li_xMo_6S_8$ delivers an areal capacity > 2.9 mAh cm^{-2} with an excellent retention of 93.1% over 100 cycles when paired with the high-sulfur-loading (4.02 mg cm^{-2}) cathode. Such an interlayer can

Please cite this article in press as: Xue et al., Manipulating Sulfur Mobility Enables Advanced Li-S Batteries, Matter (2019), https://doi.org/10.1016/j.matt.2019.07.002

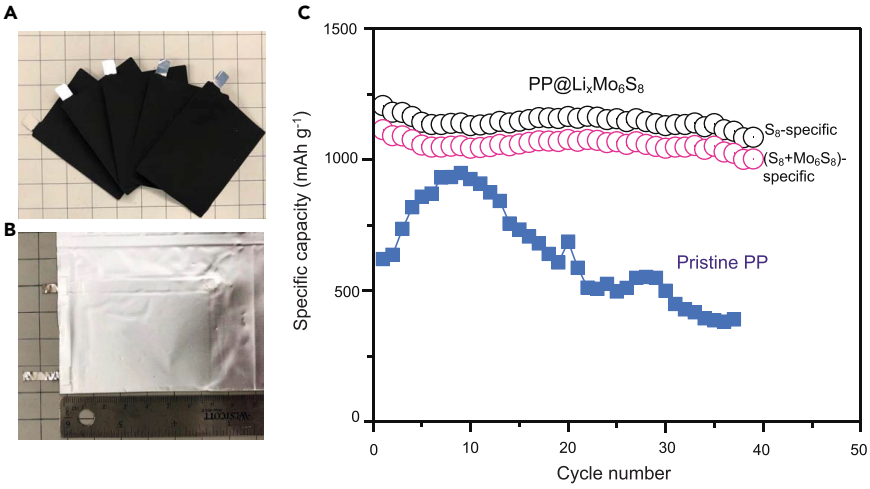

Figure 6. Electrochemical Performance of Pouch Cells

(A and B) C/S_8 cathodes with a dimension of 5.6 cm × 4.3 cm (A). (B) The pouch cell after injecting electrolyte and vacuum sealing.

(C) Cycling performance of pouch cells using the rolled ~100.5-μm-thick C/S_8 cathodes and separators with/without the PP@Li$_x$Mo$_6$S$_8$ at 0.2 C. Sulfur loading is ~3.9 mg cm^{-2} and E/S ratio is ~3.3 μL mg^{-1}. It is noted that E/(S_8 + Mo$_6$S$_8$) ratio is ~3 μL mg^{-1} , taking into account the electrochemically active Mo$_6$S$_8$ weight.

successfully solve the Li_2S clogging problem and greatly facilitate the redox kinetics. Excellent rate performance with high reversible capacities of 935 mAh g^{-1}, 819 mAh g^{-1}, and 728 mAh g^{-1} at high rates of 2 C, 3 C, and 4 C can be achieved. More importantly, it works well with calendered high-loading sulfur cathodes that greatly improve the volumetric energy density and cyclability, which is confirmed by a pouch-cell test under lean electrolyte conditions. This work overcomes major limitations associated with non-active materials for separator modification and will open new avenues for developing high-energy-density Li-S batteries.

EXPERIMENTAL PROCEDURES

Preparation of the PP@Mo$_6$S$_8$

Mo$_6$S$_8$ was prepared according to Suo et al.[41] A doctor blade-based coating method was employed to modify the PP separator. Typically, the slurry was prepared by mixing 80 wt % Mo$_6$S$_8$ powder, 10 wt % conductive carbon (Timcal Super C65 conductive carbon black), and 10 wt % PVDF with *N*-methylpyrrolidinone (NMP; Sigma-Aldrich) for 12 h. The slurry for PP@C as a control sample was prepared by mixing 80 wt % Super C65 and 20 wt % of PVDF with NMP for 12 h. Subsequently, the homogeneous slurry was cast onto one side of a Celgard PP separator (25 μm thick) with a doctor blade, followed by calendering/rolling. The coated separator was dried in an oven under vacuum at 60 °C overnight. Finally, the dried PP@Mo$_6$S$_8$ was punched into a 16-mm-diameter round disk. The mass loading on the PP@Mo$_6$S$_8$ was ~0.4 mg cm^{-2} with a thickness of ~8 μm.

Preparation of Sulfur Electrodes

A mixture of conductive carbon (Super C65) and commercial sulfur powder with a weight ratio of 4:6 was sealed in a hydrothermal reactor under Ar protection and heated to 155°C for 12 h. After cooling down to room temperature, C/S_8 composite was obtained. The slurry was fabricated by mixing 90 wt % of C/S_8 composite and 10 wt % of PVDF with NMP for 24 h. Thermogravimetric analysis measurements

Please cite this article in press as: Xue et al., Manipulating Sulfur Mobility Enables Advanced Li-S Batteries, Matter (2019), https://doi.org/10.1016/j.matt.2019.07.002

showed that there is approximately 60 wt % S_8 in the C/S_8 composite (Figure S20), corresponding to ~54 wt % S_8 in cathode. The sulfur mass loading is about 1.2–1.4 mg cm^{-2}. For the preparation of high-sulfur-loading (> 4 mg cm^{-2}) cathodes, C/S_8 composite with styrene butadiene rubber aqueous binder, and carboxymethyl cellulose binder were dispersed in deionized water in a weight ratio of 9:0.5:0.5. For the pouch-cell cathode, a wet-method[4] was used to deposit nanosulfur particles onto the carbon nanotube (CNT) and graphene (G) mixture (1.5:1 by weight, provided by Prof. Bunshi Fugetsu) based on the reaction between $Na_2S_2O_3$ and H_2SO_4. The obtained CNT/G/S_8 composite, Super C65 and LA133 binder (Chengdu Indigo Power Sources, China) in a weight ratio of 80:12:8, were vigorously mixed with a deionized water/isopropyl alcohol mixture (4:1 by weight) overnight. All the above slurries were coated onto carbon-coated Al foils using doctor blade. Finally, the electrodes were rolled, dried, and punched.

Characterizations

The microstructures were studied using scanning electron microscopy (SEM) with energy-dispersive X-ray spectroscopy (Zeiss Merlin high-resolution scanning electron microscope) and TEM (JOEL, 2010F). Phase composition was investigated by XRD (Panalytical_XPert). The sulfur content in the C/S_8 composite was measured by TG-DSC (SDT Q600) under N_2 protection. The PP@Mo_6S_8 after cycling was washed with blank electrolytes three times for further tests. The Li^+ conductivity was evaluated by EIS using an electrochemical workstation (Gamry Instruments, Reference 3000). The PP@Mo_6S_8 at different discharged states were fabricated using Li metal as a counter electrode by electrochemical lithiation to 2.3 V (PP@$Li_1Mo_6S_8$), 1.9 V (PP@$Li_3Mo_6S_8$), and 1.7 V (PP@$Li_4Mo_6S_8$) and then washed thoroughly with blank electrolytes. EIS was conducted on coin cells prepared by inserting the pristine PP separators PP@C, PP@Mo_6S_8, PP@$Li_1Mo_6S_8$, PP@$Li_3Mo_6S_8$, and PP@$Li_4Mo_6S_8$ between two blocking stainless steel electrodes with the electrolyte. The calculation methods of Li^+ conductivity and diffusion coefficient are shown in Note S2. For the observation of the Li_2S clogging, we firstly disassembled the fully discharged coin cells (to 1.7 V at 0.2 C) with PP@C and PP@$Li_xMo_6S_8$ and then washed the cathodes and separators with DME thoroughly before drying. SEM observation was then conducted on the surface of interlayers and cathodes.

In Situ 3D Tomography Using FXI Beamline at the National Synchrotron Light Source II of Brookhaven National Laboratory

Pouch-cell configuration was used for testing (Figure S21) that was imaged in transmission mode at X-ray energy of 9 keV. A volume in the middle of the cell was randomly chosen for imaging. There were 444 sample projection images acquired in angle range from −53.4° to 51.4° with 0.1 s exposure time for each image. The total tomography scan time was 52 s. A fast charge-discharge rate (~2 C) was used while collecting images for tracking electrode morphology evolution. The open-source Python package TomoPy[45] was used to reconstruct each set of images to 3D structure. The effective voxel size is 21 nm. To reduce tomography reconstruction artifacts due to missing angles from the ideal 180° angle range, we utilized a machine learning-based algorithm to post-process the reconstructed slice images.[46] A training dataset was obtained from an *ex situ* measurement of same type of electrode sample under the same scanning conditions but with a form suitable for a scan in 180° angle range. The tomography reconstructions with the training dataset with limited-angle range −53.4° to 51.4° are compared with that reconstructed from the complete dataset in 180°. The trained neural network is then applied to the reconstructions with *in situ* limited-angle data to

remove the artifacts. The 3D structure visualization in Figure 2 was done with ParaView.[47]

Electrochemical Measurements

CR2032 coin cells were fabricated with the PP@Mo_6S_8 as separator, the C/S_8 cathode and Li metal anode in a glovebox with Ar and H_2O contents <1 ppm. The pouch-cell assembly process can be found in Xue et al.[6] The lithium metal foils used in coin and pouch cells were 350 μm and 160 μm thick, respectively. 1 M lithium bis(trifluoromethanesulfonyl)imide (LiTFSI) dissolved in a mixture of DOL and DME (1:1 by volume) with 2 wt % $LiNO_3$ was used as the electrolyte for coin cells (E/S ratios for low- and high-loading sulfur cathodes are 20 and 10 μL mg^{-1}, respectively) and 0.6 M LiTFSI/0.4 M $LiNO_3$ in DOL and DME was used for pouch cells (E/S ratio is 3.3–3.4 μL mg^{-1}). Galvanostatic cycling was performed on Landt CT 2001A and Neware cyclers within 1.7–2.8 V versus Li/Li^+ at different C-rates. For coin cells, 1 C is defined as 1.672 mA mg^{-1}. For pouch cells, 1 C is denoted as the discharge current that will discharge the entire battery in 1 h at 1.7 V (100% depth of discharge). CV and EIS tests were conducted on an electrochemical workstation (Gamry Instruments, Reference 3000).

SUPPLEMENTAL INFORMATION

Supplemental Information can be found online at https://doi.org/10.1016/j.matt.2019.07.002.

ACKNOWLEDGMENTS

We would like to acknowledge the support by Samsung Advanced Institute of Technology, Wuxi Weifu Group Co., Ltd., National Key Technologies R&D Program, China (2018YFB0104400) and the National Natural Science Foundation of China (51872322). We also acknowledge Prof. Bunshi Fugetsu at School of Engineering, The University of Tokyo, for providing us the carbonaceous materials. L.S. acknowledges the One Hundred Talent Project of the Chinese Academy of Sciences and Thousand Talents Program for Young Scientists. This research used resources of the beamline FXI/18ID of the National Synchrotron Light Source II, a US Department of Energy (DOE) Office of Science User Facility operated for the DOE Office of Science by Brookhaven National Laboratory under contract no. DE-SC0012704.

AUTHOR CONTRIBUTIONS

L.S., W.X., and J.L. conceived the concept and designed the experiments; W.X. and L.S. fabricated the interlayer; W.X., M.K., C.W., and L.Q. fabricated the sulfur cathode; W.X., G.X., Y.C., Z.Z., and A.S.H. performed materials characterization and electrochemical measurements; Z.W. and D.Y. carried out the TEM observations; D.Y., X.X., M.G., and W.-K.L. conducted the *in situ* synchrotron-based 3D tomography characterization; W.X., L.S., and J.L. wrote the paper. All authors discussed the results and reviewed the manuscript.

DECLARATION OF INTERESTS

The authors declare no competing financial interests.

Received: March 7, 2019
Revised: June 9, 2019
Accepted: July 3, 2019
Published: September 4, 2019

REFERENCES

1. Manthiram, A., Fu, Y., Chung, S.H., Zu, C., and Su, Y.S. (2014). Rechargeable lithium-sulfur batteries. Chem. Rev. *114*, 11751–11787.
2. Zhang, S., Zhao, K., Zhu, T., and Li, J. (2017). Electrochemomechanical degradation of high-capacity battery electrode materials. Prog. Mater. Sci. *89*, 479–521.
3. Xue, W., Yan, Q.-B., Xu, G., Suo, L., Chen, Y., Wang, C., Wang, C.-A., and Li, J. (2017). Double-oxide sulfur host for advanced lithium-sulfur batteries. Nano Energy *38*, 12–18.
4. Liang, X., Hart, C., Pang, Q., Garsuch, A., Weiss, T., and Nazar, L.F. (2015). A highly efficient polysulfide mediator for lithium-sulfur batteries. Nat. Commun. *6*, 5682.
5. Li, Z., Zhang, J.T., Chen, Y.M., Li, J., and Lou, X.W. (2015). Pie-like electrode design for high-energy density lithium-sulfur batteries. Nat. Commun. *6*, 8850.
6. Xue, W., Shi, Z., Suo, L., Wang, C., Wang, Z., Wang, H., So, K.P., Maurano, A., Yu, D., Chen, Y., et al. (2019). Intercalation-conversion hybrid cathodes enabling Li-S full-cell architectures with jointly superior gravimetric and volumetric energy densities. Nat. Energy *4*, 374–382.
7. Liu, J., Galpaya, D.G.D., Yan, L., Sun, M., Lin, Z., Yan, C., Liang, C., and Zhang, S. (2017). Exploiting a robust biopolymer network binder for an ultrahigh-areal-capacity Li-S battery. Energy Environ. Sci. *10*, 750–755.
8. Chen, W., Qian, T., Xiong, J., Xu, N., Liu, X., Liu, J., Zhou, J., Shen, X., Yang, T., Chen, Y., et al. (2017). A new type of multifunctional polar binder: toward practical application of high energy lithium sulfur batteries. Adv. Mater. *29*, 1605160.
9. Su, Y.-S., and Manthiram, A. (2012). Lithium-sulphur batteries with a microporous carbon paper as a bifunctional interlayer. Nat. Commun. *3*, 1166.
10. Fan, L., Li, M., Li, X., Xiao, W., Chen, Z., and Lu, J. (2019). Interlayer material selection for lithium-sulfur batteries. Joule *3*, 361–386.
11. Thangavel, V., Xue, K.-H., Mammeri, Y., Quiroga, M., Mastouri, A., Guéry, C., Johansson, P., Morcrette, M., and Franco, A.A. (2016). A microstructurally resolved model for Li-S batteries assessing the impact of the cathode design on the discharge performance. J. Electrochem. Soc. *163*, A2817–A2829.
12. Huang, J.-Q., Zhuang, T.-Z., Zhang, Q., Peng, H.-J., Chen, C.-M., and Wei, F. (2015). Permselective graphene oxide membrane for highly stable and anti-self-discharge lithium-sulfur batteries. ACS Nano *9*, 3002–3011.
13. Zhou, G., Li, L., Wang, D.W., Shan, X.Y., Pei, S., Li, F., and Cheng, H.M. (2015). A flexible sulfur-graphene-polypropylene separator integrated electrode for advanced Li-S batteries. Adv. Mater. *27*, 641–647.
14. Xu, G., Kushima, A., Yuan, J., Dou, H., Xue, W., Zhang, X., Yan, X., and Li, J. (2017). Ad hoc solid electrolyte on acidized carbon nanotube paper improves cycle life of lithium-sulfur batteries. Energy Environ. Sci. *10*, 2544–2551.
15. Pang, Q., Liang, X., Kwok, C.Y., and Nazar, L.F. (2016). Advances in lithium-sulfur batteries based on multifunctional cathodes and electrolytes. Nat. Energy *1*, 16132.
16. Liu, X., Huang, J.Q., Zhang, Q., and Mai, L. (2017). Nanostructured metal oxides and sulfides for lithium-sulfur batteries. Adv. Mater. *29*, 1601759.
17. Zhou, G., Zhao, Y., Zu, C., and Manthiram, A. (2015). Free-standing TiO_2 nanowire-embedded graphene hybrid membrane for advanced Li/dissolved polysulfide batteries. Nano Energy *12*, 240–249.
18. Xu, G., Yuan, J., Tao, X., Ding, B., Dou, H., Yan, X., Xiao, Y., and Zhang, X. (2015). Absorption mechanism of carbon-nanotube paper-titanium dioxide as a multifunctional barrier material for lithium-sulfur batteries. Nano Res. *8*, 3066–3074.
19. Yim, T., Han, S.H., Park, N.H., Park, M.-S., Lee, J.H., Shin, J., Choi, J.W., Jung, Y., Jo, Y.N., Yu, J.-S., et al. (2016). Effective polysulfide rejection by dipole-aligned $BaTiO_3$ coated separator in lithium-sulfur batteries. Adv. Funct. Mater. *26*, 7817–7823.
20. Zhou, T., Lv, W., Li, J., Zhou, G., Zhao, Y., Fan, S., Liu, B., Li, B., Kang, F., and Yang, Q.-H. (2017). Twinborn TiO_2-TiN heterostructures enabling smooth trapping-diffusion-conversion of polysulfides towards ultralong life lithium-sulfur batteries. Energy Environ. Sci. *10*, 1694–1703.
21. Ghazi, Z.A., He, X., Khattak, A.M., Khan, N.A., Liang, B., Iqbal, A., Wang, J., Sin, H., Li, L., and Tang, Z. (2017). MoS_2/celgard separator as efficient polysulfide barrier for long-life lithium-sulfur batteries. Adv. Mater. *29*, 1606817.
22. Bai, S., Liu, X., Zhu, K., Wu, S., and Zhou, H. (2016). Metal-organic framework-based separator for lithium-sulfur batteries. Nat. Energy *1*, 16094.
23. Bai, S., Zhu, K., Wu, S., Wang, Y., Yi, J., Ishida, M., and Zhou, H. (2016). A long-life lithium-sulphur battery by integrating zinc-organic framework based separator. J. Mater. Chem. A *4*, 16812–16817.
24. Sun, J., Sun, Y., Pasta, M., Zhou, G., Li, Y., Liu, W., Xiong, F., and Cui, Y. (2016). Entrapment of polysulfides by a black-phosphorus-modified separator for lithium-sulfur batteries. Adv. Mater. *28*, 9797–9803.
25. Zhang, Z., Lai, Y., Zhang, Z., Zhang, K., and Li, J. (2014). Al_2O_3-coated porous separator for enhanced electrochemical performance of lithium sulfur batteries. Electrochim. Acta *129*, 55–61.
26. Yao, H., Yan, K., Li, W., Zheng, G., Kong, D., Seh, Z.W., Narasimhan, V.K., Liang, Z., and Cui, Y. (2014). Improved lithium-sulfur batteries with a conductive coating on the separator to prevent the accumulation of inactive S-related species at the cathode-separator interface. Energy Environ. Sci. *7*, 3381–3390.
27. Pang, Q., Kundu, D., Cuisinier, M., and Nazar, L.F. (2014). Surface-enhanced redox chemistry of polysulphides on a metallic and polar host for lithium-sulphur batteries. Nat. Commun. *5*, 4759.
28. Tao, X., Wang, J., Ying, Z., Cai, Q., Zheng, G., Gan, Y., Huang, H., Xia, Y., Liang, C., Zhang, W., et al. (2014). Strong sulfur binding with conducting Magneli-phase $Ti_{(n)}O_{2(n-1)}$ nanomaterials for improving lithium-sulfur batteries. Nano Lett. *14*, 5288–5294.
29. Li, Z., Zhang, J., Guan, B., Wang, D., Liu, L.-M., and Lou, X.W. (2016). A sulfur host based on titanium monoxide@carbon hollow spheres for advanced lithium–sulfur batteries. Nat. Commun. *7*, 13065.
30. Sun, Z., Zhang, J., Yin, L., Hu, G., Fang, R., Cheng, H.-M., and Li, F. (2017). Conductive porous vanadium nitride/graphene composite as chemical anchor of polysulfides for lithium-sulfur batteries. Nat. Commun. *8*, 14627.
31. Pang, Q., Kundu, D., and Nazar, L.F. (2016). A graphene-like metallic cathode host for long-life and high-loading lithium-sulfur batteries. Mater. Horiz. *3*, 130–136.
32. Xue, W., Miao, L., Qie, L., Wang, C., Li, S., Wang, J., and Li, J. (2017). Gravimetric and volumetric energy densities of lithium-sulfur batteries. Curr. Opin. Electrochem. *6*, 92–99.
33. Pope, M.A., and Aksay, I.A. (2015). Structural design of cathodes for Li-S batteries. Adv. Energy Mater. *5*, 1500124.
34. Choi, J.W., and Aurbach, D. (2016). Promise and reality of post-lithium-ion batteries with high energy densities. Nat. Rev. Mater. *1*, 16013.
35. Lv, D., Zheng, J., Li, Q., Xie, X., Ferrara, S., Nie, Z., Mehdi, L.B., Browning, N.D., Zhang, J.-G., Graff, G.L., et al. (2015). High energy density lithium sulfur batteries—challenges of thick sulfur cathodes. Adv. Energy Mater. *5*, 1402290.
36. Chang, C.H., Chung, S.H., and Manthiram, A. (2016). Effective stabilization of a high-loading sulfur cathode and a lithium-metal anode in Li-S batteries utilizing SWCNT-modulated separators. Small *12*, 174–179.
37. Yu, X., Joseph, J., and Manthiram, A. (2015). Polymer lithium-sulfur batteries with a Nafion membrane and an advanced sulfur electrode. J. Mater. Chem. A *3*, 15683–15691.
38. Balach, J., Jaumann, T., Klose, M., Oswald, S., Eckert, J., and Giebeler, L. (2015). Functional mesoporous carbon-coated separator for long-life, high-energy lithium-sulfur batteries. Adv. Funct. Mater. *25*, 5285–5291.
39. Chung, S.H., and Manthiram, A. (2014). A polyethylene glycol-supported microporous carbon coating as a polysulfide trap for utilizing pure sulfur cathodes in lithium-sulfur batteries. Adv. Mater. *26*, 7352–7357.
40. Chung, S.H., and Manthiram, A. (2014). Bifunctional separator with a light-weight carbon-coating for dynamically and statically stable lithium-sulfur batteries. Adv. Funct. Mater. *24*, 5299–5306.
41. Suo, L., Borodin, O., Gao, T., Olguin, M., Ho, J., Fan, X., Luo, C., Wang, C., and Xu, K. (2015). "Water-in-salt" electrolyte enables

high-voltage aqueous lithium-ion chemistries. Science *350*, 938–943.

42. Mei, L., Xu, J., Wei, Z., Liu, H., Li, Y., Ma, J., and Dou, S. (2017). Chevrel phase Mo_6T_8 (T = S, Se) as electrodes for advanced energy storage. Small *13*, 1701441.

43. Nitta, N., Wu, F., Lee, J.T., and Yushin, G. (2015). Li-ion battery materials: present and future. Mater. Today *18*, 252–264.

44. Cañas, N.A., Hirose, K., Pascucci, B., Wagner, N., Friedrich, K.A., and Hiesgen, R. (2013). Investigations of lithium-sulfur batteries using electrochemical impedance spectroscopy. Electrochim. Acta *97*, 42–51.

45. Gürsoy, D., De Carlo, F., Xiao, X., and Jacobsen, C. (2014). TomoPy: a framework for the analysis of synchrotron tomographic data. J. Synchrotron Radiat. *21*, 1188–1193.

46. Pelt, D., Batenburg, K., and Sethian, J. (2018). Improving tomographic reconstruction from limited data using mixed-scale dense convolutional neural networks. J. Imaging *4*, 128.

47. Ahrens, J., Geveci, B., and Law, C. (2005). Paraview: an end-user tool for large data visualization. In The Visualization Handbook, C.D. Hansen and C.R. Johnson, eds. (Academic Press), pp. 717–731.